

<https://doi.org/10.1038/s41612-024-00775-2>

Intraseasonal shift in the wintertime North Atlantic jet structure projected by CMIP6 models



Marina García-Burgos ^{1,2}✉, Blanca Ayarzagüena ¹, David Barriopedro ², Tim Woollings ³ & Ricardo García-Herrera ^{1,2}

The projected winter changes of the North Atlantic eddy-driven jet (EDJ) under climate change conditions have been extensively analysed. Previous studies have reported a squeezed and elongated EDJ. However, other changes present large uncertainties, specifically those related to the intensity and latitude. Here, the projections of the EDJ in a multimodel ensemble of CMIP6 are scrutinised by using a multiparametric description of the EDJ. The multimodel mean projects non-stationary responses of the EDJ latitude through the winter, characterised by a poleward shift in early winter and equator migration in late winter. These intraseasonal shifts (rather than a genuine narrowing) explain the previously established squeezing of the EDJ and are linked to the future changes in different drivers: the 200 hPa meridional temperature gradient and Atlantic warming hole in early winter, and the stratospheric vortex in late winter. Model biases also influence EDJ projections, contributing to the poleward shift in early winter.

The Northern Hemisphere eddy-driven jet (EDJ) is the central component of the boreal extratropical circulation and the leading regulator of weather and climate in the mid-latitudes. Due to its close relation to many tropospheric and surface processes, such as the storm track¹, regional surface weather conditions² and extreme events³, the study of future EDJ changes remains a priority. The EDJ response to an atmospheric increase of greenhouse gas (GHG) concentrations has been a topic of interest since the first phases of the Coupled Models Intercomparison Project (CMIP). A robust consensus has been found across general circulation models (GCMs) and generations on the poleward shift of the EDJ when considering annual and zonal averages^{4–8}. However, the picture changes for the winter season and the North Atlantic sector (NATL). The NATL EDJ response to climate change presents a seasonal cycle characterised by a poleward shift from spring to autumn, peaking in summer but without a clear latitudinal displacement in winter^{9,10}. Climate change projections of the EDJ latitude in winter display a large inter-model spread, spanning from poleward to equatorward responses. This behaviour has sometimes been interpreted from the multimodel mean perspective as an increasing presence of the EDJ on its central latitude in the future^{7,11,12}.

In addition to the latitudinal position, future projections indicate a strengthening of the EDJ core region with a reduction of the zonal wind on the poleward and equatorward flanks^{6,10,12}, sometimes interpreted as a

squeezing⁷. However, there is no consensus either on this reinforcement of the EDJ, as some studies find it insignificant or do not detect it^{4,9,11}. Apart from the responses in the typically studied EDJ features (latitude and intensity), changes in other aspects have also been detected. An eastward elongation over Europe^{12–14} and increased zonalization^{11,15} have been reported since early CMIP phases. However, these changes have often been inferred from the analysis of EDJ-related variables such as the zonal wind¹² or European blocking frequency^{9,16}. Finally, although some of the aforementioned studies^{12,13,16} have analysed the EDJ from a multimodel perspective, little attention has been paid to the inter-model spread, particularly for attributes other than latitude and intensity.

The uncertainties of the EDJ response to climate change are determined by multiple factors, such as changes in large-scale phenomena, and different drivers can induce different responses in the EDJ. A well-known example is the ‘tug-of-war’ between the strong upper tropospheric tropical warming (or Tropical Amplification, TA) and the rapid near-surface warming in the Arctic (i.e. the Arctic Amplification, AA). Both phenomena imply changes in the air temperature distribution, leading to a strengthening of the upper tropospheric meridional temperature gradient and a weakening of the lower one, respectively. Consequently, the TA (AA) can potentially shift the EDJ poleward (equatorward)^{17–21}. There is high confidence that both regions warm at faster rates than the global mean under GHG

¹Departamento de Física de la Tierra y Astrofísica, Universidad Complutense de Madrid, 28040 Madrid, Spain. ²Instituto de Geociencias (IGEO), CSIC-UCM, 28040 Madrid, Spain. ³Department of Physics, Atmospheric, Oceanic and Planetary Physics, University of Oxford, Parks Rd, Oxford, OX1 3PU, UK.

✉ e-mail: maring13@ucm.es

Table 1 | EDJ parameters

Mathematical expression	Description
$\text{Lat} = \max_{\phi \in [15^\circ\text{N}, 75^\circ\text{N}]} U_c(\phi)$	The latitude at which U_c attains its maximum.
$\text{Int} = U_c(\text{Lat})$	The U_c value at Lat.
$\text{Sh} = \text{Int} - \overline{U(\phi)}_c : \phi \in [15^\circ\text{N}, 75^\circ\text{N}]$	The difference between Int and the meridional mean of U_c over all latitudes $[15^\circ\text{N}, 75^\circ\text{N}]$.
$\frac{U_c(\text{Latn})}{\text{Latn} - [\text{Lat}, 75^\circ\text{N}]} = \text{Int} - \text{Sh}/2$	Latn: The latitude of the poleward flank of EDJ where U_c decreases the half of Sh.
$\frac{U_c(\text{Lats})}{\text{Lats} - [15^\circ\text{N}, \text{Lat}]} = \text{Int} - \text{Sh}/2$	As Latn but for the equatorward flank.
$\text{Til} = 60 \cdot b$ $\text{Lat}_\lambda^* \sim a + b \cdot \lambda : \lambda \in [60^\circ\text{W}, 0^\circ]$	The slope of the tracked latitudes (Lat_λ^*) of Lat along the NATL.
$\text{Lon} = \sum_{\lambda=60^\circ\text{W}}^0 \lambda \cdot \text{Int}_\lambda^2 / \sum_{\lambda=60^\circ\text{W}}^0 \text{Int}_\lambda^2$	The average of the NATL longitudes weighted by the square of Int_λ (the zonal wind at Lat_λ^*).
$[\text{Lonw}, \text{Lone}] \in [90^\circ\text{W}, 30^\circ\text{E}] : \Delta \text{Int}_{[\text{Lonw}, \text{Lone}]} \geq 0.5 \cdot \Delta \text{Int}_{[60^\circ\text{W}, 0^\circ]}$	The longitudinal interval $[\text{Lonw}, \text{Lone}]$ around Lon containing half of the Int_λ contours over the NATL.
$\text{Dep} = \sqrt{\frac{\sum_{\lambda=60^\circ\text{W}}^0 (\text{Lat}_\lambda - \text{Lat}_\lambda^*)^2}{n}}$	The spread in the location of the latitudinal wind maxima (Lat_λ) obtained for the n longitudinal sectors of the NATL with respect to the fitted Lat_λ^* .

Mathematical expressions synthesising the computation of the EDJ parameters (left column) and a brief explanation (right column). The zonal mean of $u850$ averaged over a longitudinal sector of 60° width is denoted by U_λ , with λ indicating the half longitude of the sector (the subindex c refers to the centre of the NATL sector, i.e. $\lambda = 30^\circ\text{W}$). The latitudes are represented by ϕ . The intercept and slope of the linear regression are denoted by a and b . Lat_λ^* depicts the latitudes obtained from the zonal tracking of the latitudinal peak Lat over the U_λ profiles of the NATL sector, so that contiguous values cannot differ by more than 5° . Lat_λ identifies the latitudes of the wind peak in U_λ , which do not necessarily coincide with Lat_λ^* . See the “Methods” section for details.

increases^{6,22,23}. As TA and AA act simultaneously, the combined effect can result in poleward or equatorward EDJ migrations, depending on which one dominates. In turn, these EDJ migrations can lead to further changes in the meridional gradients²⁴.

Something similar happens for the projected changes in sea surface temperature (SST). There is a large agreement across GCM projections about a global heterogeneous warming of the oceans, particularly more pronounced in the tropics and Northern Hemisphere²⁵. However, this generalised warming exhibits a striking anomaly in the NATL ocean. Projections of the NATL subpolar gyre region indicate a lack of warming or even a cooling, a feature known as the NATL Warming Hole (WH)²⁶. The NATL WH modifies the baroclinicity over the western basin, which can affect the storm tracks and the EDJ latitude and intensity through thermal wind responses^{26,27}. An EDJ eastward extension has also been linked to the baroclinicity strengthening^{13,28,29}. Although the NATL WH is a robust aspect of climate change, the magnitude of the change presents a large spread across GCMs, which propagates to the EDJ response²⁹.

The uncertainties of the EDJ projections further increase when not only the magnitude but also the sign of the driver’s response to climate change is uncertain. For instance, the stratospheric polar vortex (SPV), whose intensity also modulates the EDJ latitude and intensity^{30,31}, is projected to reinforce or weaken under increasing GHG concentrations depending on the GCM^{32,33}. Changes in the longitudinal SST gradients of the tropical Pacific can also affect the mid-latitude NATL circulation through Rossby waves and teleconnections^{34,35}. The sign of SST gradients determines the location of the wave source along the tropical Pacific, potentially affecting the position and structure of the EDJ³⁵.

Non-stationary signals in the drivers or the background flow through the winter would further increase the uncertainty of EDJ projections by inducing seasonally varying responses. For the tropical Pacific SST, it is well established that the teleconnections linking the Pacific and Atlantic basins are different in early and late winter, yielding intraseasonal influences on the EDJ^{36–39}. Little attention has been given to studying intraseasonal responses of the NATL circulation⁴⁰. Finally, the presence of biases in GCMs is an additional source of uncertainty. For example, GCMs often present systematic biases in the representation of the EDJ latitudinal position, which tends to be equatorward shifted compared to observations^{4,41}. This may potentially contribute to the spread in the projections of the NATL circulation¹⁰.

In this paper, we describe the climate change projections of the winter NATL EDJ in the last generation of climate models (CMIP6). The uncertainties of the EDJ projections are related to those of well-known drivers. To do so, we use a novel approach presented by Barriopedro et al., (2023)⁴², which describes the EDJ from a multiparametric perspective. For each day, the method provides (i) a suite of ten parameters, each of them quantifying a specific aspect of the EDJ structure; (ii) a 2D detection of the EDJ (i.e., grid points comprising the zonal wind maxima over the NATL). The latter provides an explicit spatial representation of the EDJ and enables the computation of maps with the spatial frequency of EDJ occurrence over a given time interval. A detailed description of the EDJ parameters, the 2D EDJ frequency field and their computation based on the NATL lower tropospheric zonal wind are provided in the Methods section (see Jet parameters subsection and Table 1 for a summary). We find that the EDJ latitudes do not show consistent changes across the whole winter in a multimodel ensemble of future projections, but opposite intraseasonal meridional shifts. The mixture of contrasting signals in early and late winter reflects different influences from thermodynamical (meridional temperature gradient at 200hPa) and dynamical (SPV) responses to climate change. Moreover, equatorward GCM biases also contribute to the intraseasonal differences in latitudinal shifting by enhancing the poleward migration during the whole season.

Results

Seasonal analysis of projections

Figure 1 shows the multimodel mean future change in the frequency of occurrence of EDJ during the extended winter (November-to-February, NDJF). The spatial pattern features a tripolar structure, which resembles a squeezing of the climatological EDJ, depicted by an intensification of its central part and a weakening of the northern and southern flanks (Fig. 1a). A similar pattern is found for the 850 hPa zonal wind but with noisier characteristics (Fig. S1). The tripolar pattern in Fig. 1a does not necessarily imply a change in the latitudinal position (Lat) or intensity (Int) of the EDJ in the future, as shown by the distributions of the changes in the corresponding parameters (see the grey whiskers for Lat and Int in Fig. 1b), which are centred around the zero-line. The similarity of the Lat distributions in both future and historical periods (Fig. S2a) confirms the lack of changes in the latitudinal position of the EDJ (Fig. 1a).

The tripolar pattern influences the EDJ zonality, herein represented by the Departure (Dep) parameter, which measures the deviation of the EDJ

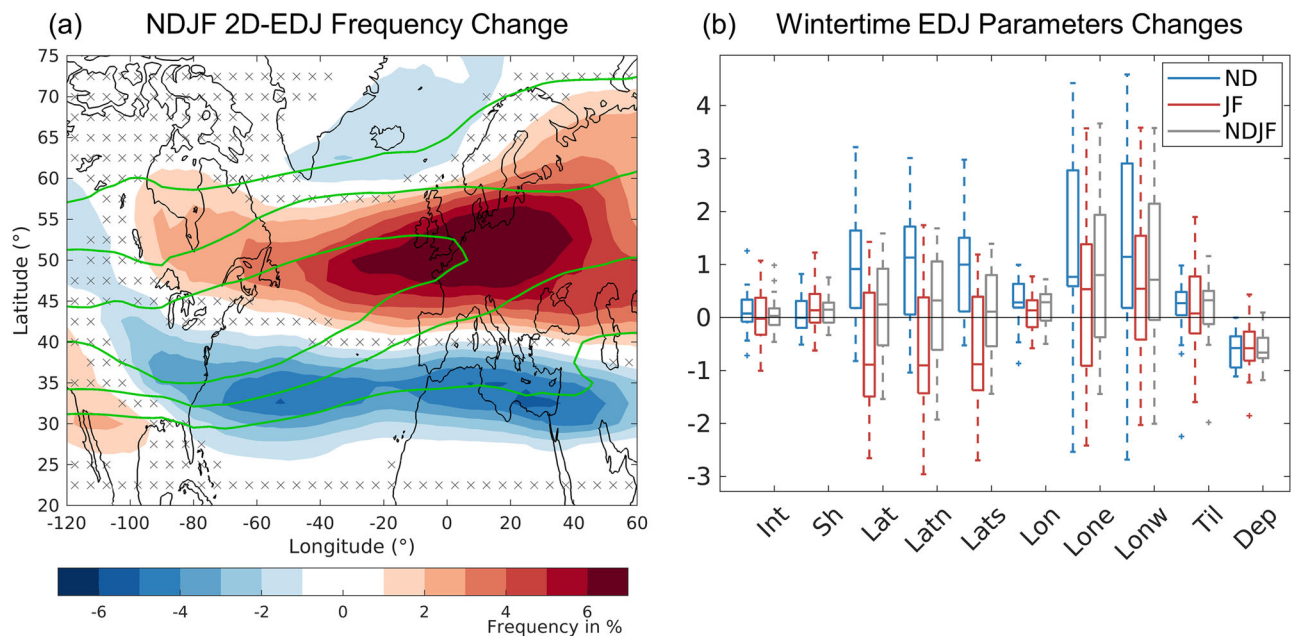


Fig. 1 | Winter projections of the EDJ. **a** Multimodel mean climate change signal in the winter (NDJF) 2D EDJ frequency (shading, [%]). The 1979–2009 NDJF climatology is shown with green contours (starting at 20% and drawn every 20%). Crosses indicate the grid-points with non-significant differences at the 95% confidence level (after a 1000-trial Monte Carlo test). **b** Boxplots with the future changes in the EDJ parameters (Int, Sh [m/s]; Lat, Latn, Lats [°N]; Lon, Lone, Lonw [°E]; Til, Dep [°N/

60°]) for NDJF (grey), ND (blue) and (JF) red. The distance between the box limits denotes the interquartile range and the horizontal line corresponds to the median. Whiskers indicate the extremes of the distribution without considering outliers. Outliers, defined as values >1.5 times the interquartile range, are represented with crosses. The climate change signal is defined as the difference between future (2069–99; SSP5–8.5) and present-day (1979–2009; historical) means.

from a structure with a single wind maximum. Large values of this parameter indicate a split-like pattern with two or more wind maxima. GCMs project a robust increase in zonality and a tendency towards EDJs with a single flow configuration since the distribution of the Dep changes is displaced toward negative values. This is consistent with the increased frequency of winter days with EDJ over western Europe (Fig. 1a). An eastward displacement of the EDJ is also captured by the projected changes in the longitudinal parameters (Lon, Lone and Lonw; Fig. 1b), although the associated spread is large, spanning from negative (westward) to positive (eastward) values.

Despite the general consistency of the future changes in the EDJ parameters and 2D EDJ frequency, the apparent squeezing shown by the latter (Fig. 1a) and several works^{6,7,11,15} is not detected in the analysis of the EDJ parameters (Fig. 1b). This emphasises the complementary information provided by these two EDJ perspectives and calls for caution when interpreting changes in zonal wind and/or 2D EDJ frequency. In particular, the tripolar pattern of Fig. 1a allows various interpretations, since changes in different EDJ features can lead to the same pattern. The combined analysis of the 2D EDJ frequency and the EDJ parameters provides a more complete view of the EDJ, making it possible to deepen into its complex structure. In this sense, the parameter Sh measures the sharpness of the EDJ and can be taken as an indicator of the squeezing, with a narrowing and widening of the EDJ translating to positive and negative changes in Sh, respectively. The median of the multimodel changes of Sh indicates a slight narrowing, in agreement with all the above-mentioned previous works. However, our parametric approach also reveals a large uncertainty (non-significant narrowing): the distribution of the changes is centred around the zero line, ranging from positive to negative values. Alternatively, the apparent squeezing pattern of Fig. 1a might be understood as sole changes in the latitudinal frequency, involving more frequent central EDJs and less poleward and equatorward excursions, but without changes in the EDJ width. However, as previously mentioned, Lat and Int parameters do not show clear changes in the future either (Figs. 1b and S2). Thus, none of the interpretations of the spatial pattern depicted by the 2D EDJ frequency is supported by the future changes in EDJ parameters.

Considering the mentioned consensus on the projected squeezing of the EDJ^{6,7,11,15} and the strong impacts of the EDJ on European regional climates and extreme events^{42,43}, the mismatch between the projected changes retrieved from the two EDJ perspectives (2D EDJ frequency pattern and EDJ parameters) needs to be reconciled. One possible explanation for the apparent inconsistency is that the squeezing is the result of including in the same analysis elements that are responding differently to climate change. One of these elements might be the consideration of the NDJF as a whole, given that the signals of certain EDJ drivers, such as the SPV or the equatorial Pacific SSTs, are not stationary during the winter. The next section presents the EDJ projections for the early (ND) and late (JF) winter separately, in order to address the aforementioned inconsistency and further dissect the spread in the EDJ projections.

Subseasonal analysis of projections

The projected changes in the pattern of 2D EDJ frequency (Fig. 2a, c) and distribution of EDJ parameters (coloured whiskers in Fig. 1b) show large intraseasonal variations and notable differences between ND and JF winter. Considering the EDJ width (Sh parameter), the corresponding distributions for ND and JF (Fig. 1b) do not show appreciable changes, similarly to NDJF. However, this is now consistent with the two subseasonal EDJ frequency maps, neither of which show a squeezing-like pattern (Fig. 2a, c). Note that in both subseasons, the change in the 2D EDJ frequency is dominated by a dipole pattern, indicating meridional shifts rather than changes in the EDJ width over the NATL sector.

More interestingly, the early winter EDJ shows a statistically significant displacement to the pole, to the east and toward positive tilts (a higher SW-NE orientation of the EDJ) (Fig. 2a and blue whiskers in Fig. 1b; note that the interquartile range for the associated EDJ parameters of Lat, Lon and Til does not include zero). The poleward shift can also be clearly seen in the two meridional flanks of the EDJ (Latn, Lats), confirming the absence of changes in the EDJ width, as well as in the NATL zonal wind cross section (Fig. 2b, poleward peak in Fig. S2b). Differently, the late winter EDJ does not show such changes but, if any, a tendency to be southward displaced (equatorward peaks in Fig. S2c),

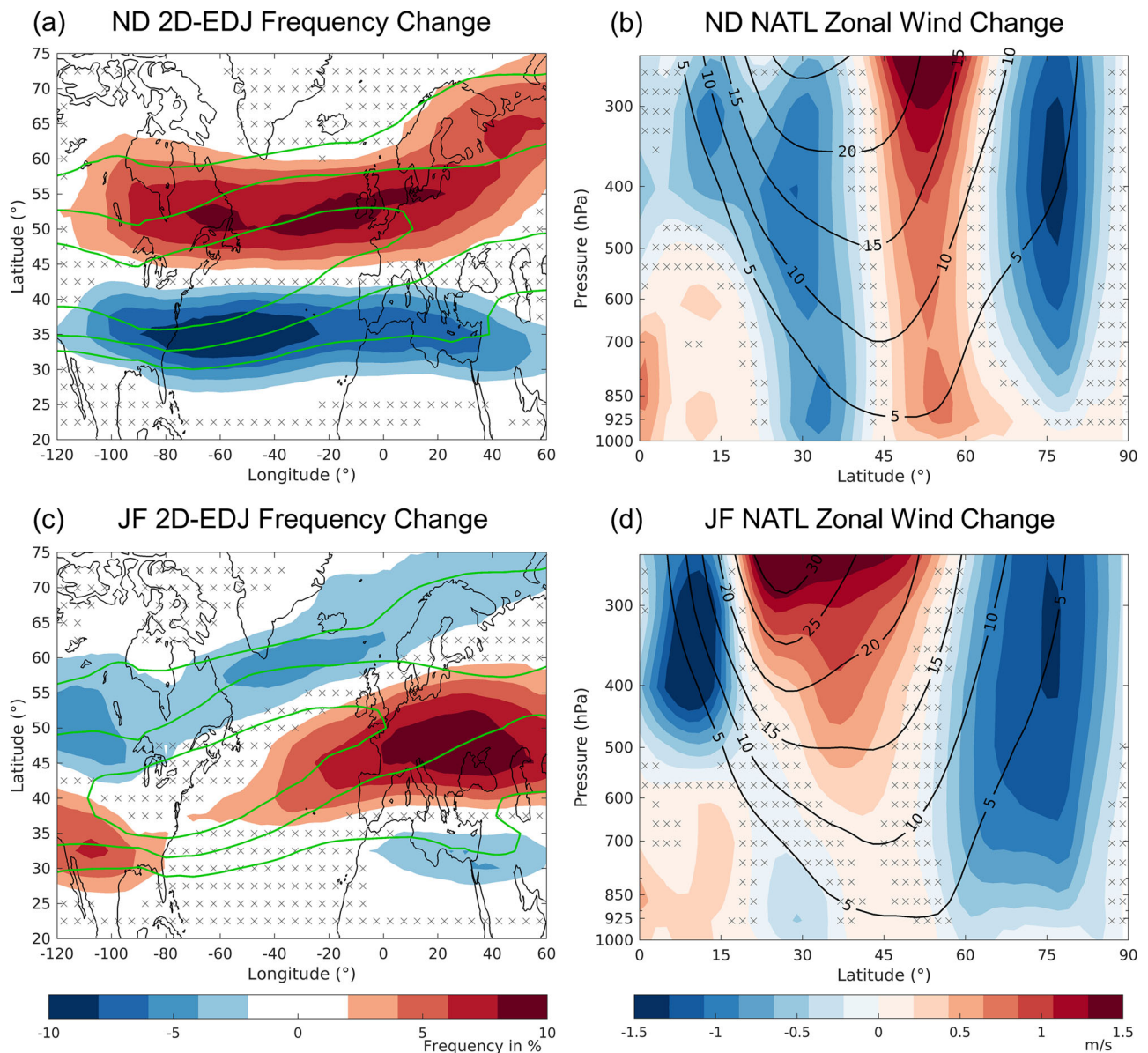


Fig. 2 | Projections of the EDJ for early and late winter. **a** and **c** As Fig. 1a but for early (ND; **a**) and late (JF; **c**) winter. **b** and **d** Multimodel mean of the future (2069–99) minus present-day (1979–2009) difference in the zonal wind averaged

over the NATL. Crosses indicate the grid-points with non-significant differences at the 95% confidence level (after a 1000-trial Monte Carlo test).

although this equatorward shift is not very well captured in the cross-section of Fig. 2d. The reason is that the EDJ is tilted in the NATL, therefore presenting positive and negative frequency changes at the same latitude (Fig. 2c). As a consequence, the signal weakens when the longitudinal average is computed over the NATL (Fig. 2d). Like in early winter, the distributions of longitudinal parameters continue to display an eastward EDJ shift in late winter. However, there are marked differences in uncertainty: during ND, there is a high model agreement on the EDJ elongation over Europe, whereas the distribution of the JF changes presents a large spread and, hence, an uncertain projection.

Out of the ten EDJ parameters, only the latitudinal ones (Lat, Latn and Lats) present significant changes in early and late winter, but of opposite sign. The latitudinal parameters are the most salient features of the NATL EDJ and they explain most of its variability. Indeed, the EDJ latitudinal shift is the primary mode of variability of the NATL zonal wind⁴⁴. Besides, the changes in the latitudinal parameters are consistent with those found for the 2D EDJ frequency. Therefore, from now on, we will focus on the projections

of the EDJ latitude (Lat) and the cause of its opposite responses to climate change in early and late winter.

Projections of the subseasonal temperature and zonal wind mean state

To understand the intraseasonal change in EDJ latitudes, we assess the future changes in the mean state of NATL zonal mean temperature (T), zonal mean zonal wind (U) and SSTs (Fig. 3). The climate change pattern of T is characterised by a stratospheric cooling and a tropospheric warming, the latter being dominated by the TA and AA throughout the entire winter (Fig. 3a, d). The main intraseasonal difference is that the change in T at upper levels and polar latitudes is not statistically significant in late winter (Fig. 3d), suggesting that the intensification of the negative meridional temperature gradient at 200 hPa is stronger in early than in late winter. On the other hand, the SST changes display very similar characteristics in both subseasons (Fig. 3b, e): besides the NATL WH, longitudinal asymmetric warming is present in the equatorial Pacific, leading to a weakening of the

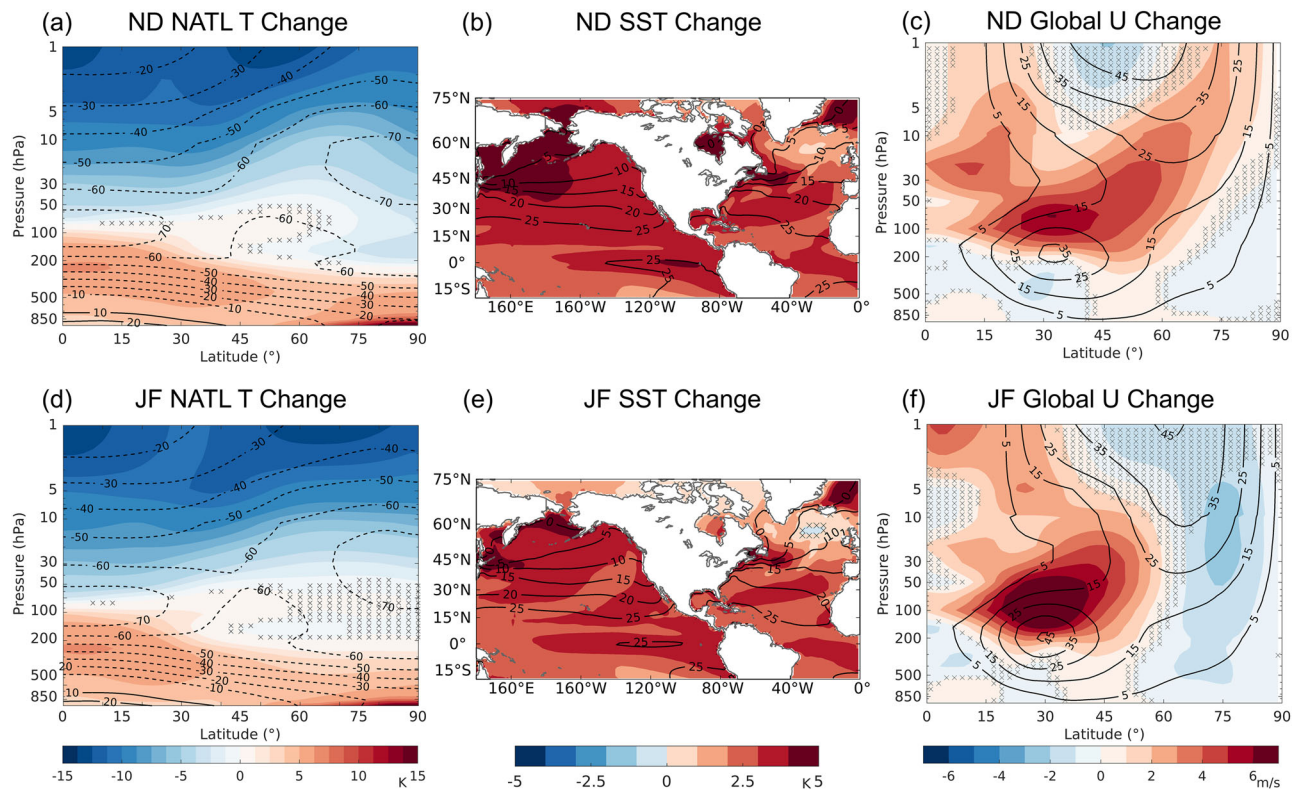


Fig. 3 | Climate change projections of temperature, SST and zonal wind. Multi-model mean future changes (shading) and 1979–2009 climatology (contour) of the zonal mean T over the NATL [K] (**a, d**), SST [K] (**b, e**) and hemispheric zonal mean U [m/s] (**c, f**). The future (2069–2099; SSP5–8.5) minus present-day (1979–2009)

differences are computed for early (upper row) and late (bottom row) winter separately. Crosses indicate the grid-points with non-significant differences at the 95% confidence level (after a 1000-trial Monte Carlo test).

longitudinal SST gradient between the western and eastern edges of the basin.

Moving to the zonal mean zonal wind changes, a reinforced subtropical jet is observed in both subseasons (Fig. 3c, f). Moreover, the maximum wind speeds are located at higher levels than in the historical period, which is consistent with the expansion of the troposphere and the subsequent rise of the tropopause^{23,45}. Note that in Fig. 3c and f, the latitudinal shifts of the NATL EDJ are masked by the zonal mean (the zonal wind is averaged globally). Interestingly, the stratospheric zonal wind response to climate change in extratropical latitudes differs between subseasons. Early winter displays an intensification of the zonal wind at polar latitudes and stratospheric levels, which expands from the subtropical jet (Fig. 3c). The reinforcement of the zonal wind in the polar stratosphere does not extend to tropospheric levels, though suggesting that the changes in the two atmospheric layers are not coupled in this case. Late winter shows a very different picture (Fig. 3f). Contrary to the early winter case, the SPV weakens in late winter, and the stratospheric and tropospheric changes are coupled since the zonal wind weakening is vertically continuous along the atmospheric column. Late winter is also the typical timing of the strongest stratosphere–troposphere coupling⁴⁶. Therefore, our results suggest a potential influence of the stratospheric future changes on the troposphere (and the EDJ) in late winter only.

In the following section we explore the linkages between the projected changes in the EDJ and its drivers (atmospheric and oceanic mean states) in order to explain the intraseasonal differences in the latitudinal shift of the EDJ. To simplify the analysis, we consider some of the aforementioned drivers of the EDJ reported in the literature, including the meridional temperature gradient at 200 hPa (Grad200) and 850 hPa (Grad850), the NATL WH, the SPV and the zonal asymmetries in the equatorial Pacific SST (see the “Methods” section). The chosen phenomena are well-established drivers of the EDJ and capture the most

relevant signatures of the atmospheric and oceanic changes identified in Fig. 3.

Drivers of the intraseasonal future changes in EDJ latitude

Early winter. Starting with early winter, we use the regression framework described in Eqs. (1) and (2) of the Methods section to model the dependence of the latitudinal EDJ parameters and the NATL atmospheric circulation on the response of the remote drivers to climate change. The multiple linear regression (MLR) identifies Grad200 and WH as the main large-scale drivers of the future changes in the early winter EDJ latitude (ΔLat). GCM biases of the EDJ latitude also have an influence. The three mentioned drivers explain together 72% of the ΔLat variance simulated by the multimodel ensemble (Grad200 explains 18%, WH 33% and the GCM biases 21% of the ΔLat variance). Similar explained variances are obtained for Latn and Lats as they are correlated with Lat. The influence of the drivers’ responses on the projected changes in EDJ frequency is shown in Fig. 4. For all drivers, their climate change fingerprints induce a meridional dipole in the EDJ extending along the NATL. Grad200 is expected to decrease further, which implies a strengthening of the (negative) meridional temperature gradient. A deeper Grad200 is expected to move the EDJ poleward (Fig. 4a). The WH directly affects the location of the strongest baroclinicity in the NATL²⁶. As the WH deepens, the region of no warming also has a larger extension. In that case, the southern edge of the deep WHs reaches lower latitudes, shifting the baroclinicity region and the EDJ equatorward (Fig. 4b). Contrary, shallow WH would indicate a small warming in that area, but still weaker than in the rest of the NATL. This would confine the WH at very high latitudes, which in turn would push the baroclinicity and EDJ poleward.

Finally, the historical biases in the EDJ latitude influence its response to climate change, especially in the southern flank of the EDJ (Fig. 4c). The

Fig. 4 | Contributions of future changes in EDJ Lat drivers to the early winter (ND) EDJ response to climate change. a EDJ frequency response (scaled by global warming) [%/K] to a + 1 sigma future change in Grad200. Green contours show the multimodel mean climatology of the 1979–2009 period (starting at 20% and drawn every 30%). Stippling indicates significance at the 95% confidence level (i.e. local regression coefficients of the corresponding driver that are significantly different from zero). **b** Same as (a) but for the NATL WH. **c** Same as (a) but for the Lat EDJ Bias. **d** Same as Fig. 1b but for Neutral-GCMs (see the “Methods” section).

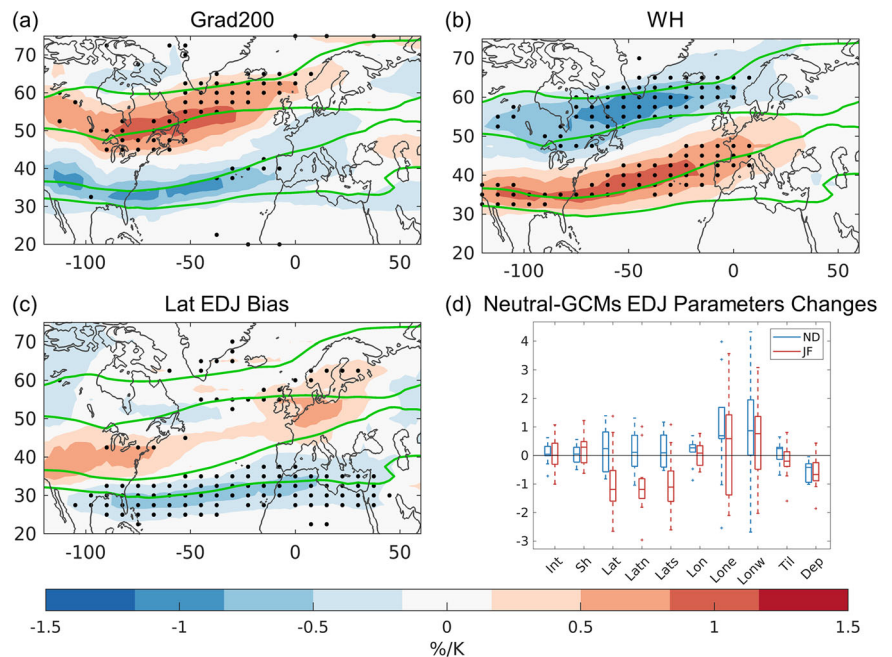
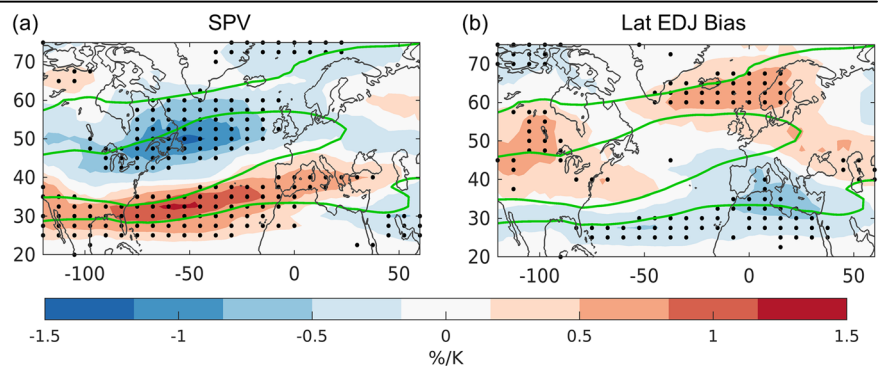


Fig. 5 | Contributions of future changes in EDJ Lat drivers to the late winter (JF) EDJ response to climate change. Same as Fig. 4a but for the drivers of EDJ latitude in late winter (JF).



dipole pattern of Fig. 4c indicates that equatorward biased GCMs (i.e. with a negative Lat EDJ bias) display more poleward shifted EDJs in the future than the unbiased (Neutral-GCMs) ones. There are 11 GCMs with a significant bias in EDJ Lat (Biased-GCMs), out of the 21 GCMs of the multimodel ensemble (see Methods), and all of them present a southward shifted EDJ in the historical period (Fig. S3a and c). Therefore, the contribution of GCM biases to the multimodel EDJ response to climate change consists of a poleward shift of the EDJ. In fact, if we analyse the projected changes in the latitudinal parameters for the Neutral-GCMs sample, the poleward displacement of the EDJ is no longer present in early winter (blue boxplots in Fig. 4d), and there is no meridional shift in the EDJ projections. These results show that at least part of the detected poleward migration of the EDJ under climate change scenarios can be a consequence of the GCM biases. For Neutral-GCMs, the biases in EDJ latitude are small and the other drivers (Grad200 and WH) explain most (~90%) of the spread in Δ Lat, with ~27% of the variance corresponding to Grad200 and ~63% to WH. As the climate change responses in Grad200 and WH involve opposite changes in the EDJ latitude, Neutral-GCM projections reflect the competing effects of these two drivers. This explains the lack of agreement in the sign of the early winter latitudinal EDJ parameters in Fig. 4d.

Late winter. The picture changes when assessing the drivers of the changes in EDJ latitude for late winter. In this case, our regression

approach indicates that the multimodel spread in Δ Lat is largely explained by only one large-scale driver, the SPV. A weakening of the SPV is associated with an equatorward shift of the EDJ (Fig. 5a), as expected from the stratosphere-troposphere coupling⁴⁶. The projections of SPV and EDJ in late winter show a consistent picture: in the future, the SPV weakens (Fig. 3f) and the EDJ shifts equatorward (see also the red boxplot in Fig. 1b). For this subseason, the bias in EDJ latitude is again found to influence Δ Lat. The spatial pattern is similar to the ND one, but with the meridional dipole more defined and displaced to the east (Fig. 5b). Like in early winter, all Biased-GCMs are shifted equatorward, contributing to a poleward shift of the EDJ that opposes the equatorward shift induced by the weakening of the SPV. The SPV, together with the Lat EDJ Bias, explains half of the total variance in Δ Lat. For the Neutral-GCMs subsample, the SPV is the only driver influencing the EDJ latitudinal response to climate change (~50% of the explained variance). In addition, the consensus on the equatorward shift detected in the multimodel ensemble is stronger in the Neutral-GCMs sample (compare Fig. 1b vs. Fig. 4d). Therefore, the results for late winter reinforce the fact that the projected poleward migration of the EDJ can be substantially driven by GCM biases. Note that future changes in the other drivers (equatorial Pacific SST and Grad850) have negligible influences on EDJ latitude for both early and late winter.

Discussion

In this paper, we have described the future winter changes of the North Atlantic (NATL) eddy-driven jet (EDJ) in the last generation of general circulation models (GCMs) by exploiting a novel daily description of the EDJ, which relies on two complementary approaches: an explicit 2D diagnosis and a multiparametric description of the complex EDJ structure.

Although there is consensus on the future poleward shift of the EDJ at hemispheric scales, several studies did not find clear latitudinal migrations in the NATL. Instead, a large spread in the projections of EDJ latitude has been detected across GCMs, ranging from poleward to equatorward displacements^{6,9}. Other studies report that the lack of a robust EDJ response to climate change is due to opposing effects of two drivers of the NATL EDJ, the Tropical (TA) and Arctic (AA) amplifications, which result in small net changes in latitude, but a pronounced squeezing of the EDJ^{6,9}. However, our results indicate that the future squeezing pattern of the winter EDJ could be an artefact from mixing different intraseasonal EDJ responses to climate change that involve opposite meridional shifts of the EDJ. By splitting the winter (November-to-February, NDJF) into two subperiods, we find a high model agreement on a poleward EDJ shift in early winter (ND), followed by a slight equatorward shift in late winter (JF). In fact, when we diagnose changes in the EDJ width explicitly, we do not find significant changes towards narrower or wider EDJs in the future, not even in early and late winter. Indeed, the apparent winter squeezing evidenced in the zonal wind and 2D EDJ frequency maps is no longer present when the EDJ changes are computed for early and late winter separately. Therefore, the effect of combining the two winter subseasons is two-fold: it yields a disproportionate increase in the uncertainty of the projections of the EDJ parameters, and a misleading response of the EDJ due to averaging opposite signals that occur at different times of the winter.

The intraseasonal latitudinal responses of the EDJ to climate change are shown to be promoted by different drivers: the upper tropospheric temperature meridional gradient (Grad200) and the NATL sea surface temperature (SST) warming hole (WH) in early winter, and the stratospheric polar vortex (SPV) in late winter. This means that the processes that drive the future changes in the EDJ latitude change throughout the winter from thermodynamic to dynamic processes. In particular, the strong influence of the SPV on the EDJ latitudes in late winter outweighs the effect of other active drivers of this subseason³², such as Grad200 and NATL WH. According to our regression model, SPV, and not the AA, represented herein as the low tropospheric temperature gradient (Grad850), would be the main responsible for the projected equatorward shifts of the EDJ, albeit limited to late winter. Therefore, the drivers of the ‘tug-of-war’ could be different (or at least should be expanded) from those previously thought. The stratosphere-troposphere coupling is typically stronger in late than in early winter, which could explain why the SPV plays an active role in the JF period but not in ND. Although some authors have linked AA to an equatorward shift of the EDJ^{9,17,18,47}, more recent studies, such as Zappa and Shepherd (2017)³³ have not found a significant impact of the AA on the zonal wind across the NATL region.

GCM biases in the EDJ latitude also influence its projections. GCMs simulating an equatorward-shifted EDJ in the historical period project a larger poleward shift of the EDJ in the future than unbiased GCMs. Indeed, when analysing the sample formed by the GCMs without biases in the EDJ latitude, the projections present no clear shift of the EDJ in early winter and a strong displacement towards the equator in late winter. This suggests that part of the projected poleward shift of the EDJ under climate change could be exacerbated by the GCM biases. One may speculate about the underlying mechanism for this influence. The answer could be found in the relative location of the EDJ to the tropical warming. Experiments carried out with idealised GCMs have shown that tropical warming forces a poleward shift of the EDJ through eddy heat and momentum fluxes¹⁸. More recently, Baker et al. (2017, 2018)^{48,49} have designed a set of experiments to study the sensitivity of the EDJ to different warming locations and intensities. They found that the poleward displacement of the EDJ was driven by warming sources

situated at its equatorial flank, with larger tropical warmings inducing larger poleward shifts. Accordingly, Biased-GCMs, which are equatorward shifted in present-day conditions, would exhibit larger poleward shifts in the future than Neutral-GCMs, since their EDJs are closer to the equator and experience greater warming on their equatorial flank.

In summary, the multiparametric perspective of the EDJ has provided a better understanding of the winter EDJ responses to climate change, allowing us to question some established changes like the EDJ squeezing, disentangle the ambiguous latitudinal EDJ responses and identify the key role of GCM biases. Furthermore, the use of the EDJ parameters together with the multiple linear regression (MLR) framework has enabled the identification of the major drivers of the future changes in the EDJ latitude, and the quantification of their relative roles and spatial fingerprints, facilitating the interpretation of the mechanisms behind the intraseasonal latitudinal shifts. Although useful, our approach also presents some drawbacks. For instance, the EDJ detection method does not account for multiple EDJs and their associated latitudes. This restriction might affect the latitudinal projections, although the effects should be small because multiple EDJs are relatively uncommon. The MLR framework also presents some limitations because it only captures the linear relations between the drivers’ responses and future EDJ changes, but not more complex behaviours such as asymmetric or non-linear responses to the drivers’ changes or eventual interactions among the drivers. Unravelling the potential dependencies among the drivers and their non-linear effects on the EDJ could further improve the assessment of the uncertainties in regional climate change projections.

The multiparametric EDJ perspective could also shed some light on other interesting, albeit less controversial, topics that remain for future work, such as the eastward displacement of the EDJ over Europe and the tendency towards EDJs with a single flow configuration. The occurrence of more zonal and eastward displaced EDJs in the future is consistent with projected decreases in European blocking^{9,50}, although feedbacks between the eddies and the mean flow prevent separating cause and effect. Finally, our approach could, in principle, be extended to analyse future projections of the EDJ in other seasons, including the summer EDJ, which has been linked to recent changes in the NATL atmospheric circulation and an unprecedented increase in the frequency of extreme events⁵¹.

Methods

In this study, we use the output of historical and SSP5–8.5 simulations from the 6th phase of the Coupled Model Intercomparison Project (CMIP6⁵²). Our multimodel ensemble is formed by one member of 21 global climate models (GCMs), listed in Table S1. The climate change signal is defined as the difference of the climatological means computed over two 30-year periods with different levels of anthropogenic forcings: 1979–2009 of the historical and 2069–2099 of the SSP5–8.5 runs. For each year of these periods, we compute time averages over the winter (November-to-February, NDJF) season and its two halves, i.e. early (ND) and late (JF) winter. The considered variables include daily zonal wind at 850 hPa (u_{850}), monthly means of zonal wind (U) and air temperature (T) at different pressure levels, and sea surface temperature (SST). For model evaluation, we use the ERA5 reanalysis⁵³. Model data and ERA5 have been linearly interpolated to the same regular $2.5^\circ \times 2.5^\circ$ grid before performing additional computations.

Jet parameters

The new method presented by Barriopedro et al. (2023)⁴² is used to characterise the eddy-driven jet (EDJ) on a daily scale. The EDJ is described by ten daily parameters computed from the 10-day low-pass filtered u_{850} . The set is formed by two categories of parameters. The basic ones are derived from the meridional profile of the zonal wind averaged over the NATL sector ($[60^\circ\text{W}, 0^\circ]$), U :

- The latitudinal position (Lat) and intensity (Int) are similar to those introduced by Woollings et al. (2010)⁴⁴ (see Table 1).
- Sharpness (Sh) measures how steep the zonal wind peak is.

- Poleward (Latn) and equatorward (Lats) flanks, located at either side of Lat, identify the meridional boundaries of the EDJ.

The remaining parameters employ additional meridional profiles (U_λ), which are computed as running means of the zonal wind over longitudinal windows of 60° width centred at each longitude λ of the $[90^\circ\text{W}, 30^\circ\text{E}]$ sector. These parameters refer to specific attributes of the 2D zonal wind structure detected by Lat. This structure is defined by the pairs $(\text{Lat}^*_\lambda, \text{Int}_\lambda)$, which are obtained by zonally tracking the latitudinal peak Lat (detected in $U_c \equiv U_{30\text{W}}$) over the contiguous U_λ profiles of the NATL sector. The search of Lat^*_λ is constrained so that Lat^*_λ values at contiguous longitudes do not fall apart by more than 5° . Note that the so-tracked latitudes Lat^*_λ do not necessarily coincide with Lat_λ , which are the latitudes of maximum U_λ within the $[15^\circ\text{N}, 75^\circ\text{N}]$ band.

- Tilt (Til) quantifies the slope of the zonal wind maxima along the NATL. Positive (negative) values indicate SW–NE (NW–SE) tilts.
- Longitudinal position (Lon) indicates whether the zonal wind maxima are larger over the eastern or western NATL.
- Westward (Lonw) and eastward (Lone) extensions inform on zonal elongations of the EDJ by detecting its outermost regions of influence (i.e. the longitudes where the zonal gradient of zonal wind is the largest).
- Departure (Dep) measures the spread of the latitudinal positions of the zonal wind maxima detected across the NATL, therefore quantifying the extent to which the EDJ presents multiple branches (split-like pattern) or a single continuous structure. High values indicate large spread and hence the presence of multiple zonal wind maxima.

In order to facilitate the interpretation of the EDJ parameters, Table 1 describes the equations employed in their computation, along with a brief explanation. The method also provides a daily 2D detection of the EDJ, which relies on the identification of Latn and Lats for each longitudinal sector U_λ of the $[120^\circ\text{W}, 60^\circ\text{E}]$ domain (hereafter Latn_λ and Lats_λ). The EDJ is defined as the grid points lying between Latn_λ and Lats_λ (the latitudinal flanks of Lat_λ). Labelling them with ones and the rest with zeros, we generate a binary field describing the 2D structure of the EDJ. The daily binary fields of a given time interval can be employed to obtain 2D maps with the local frequency of EDJ occurrence. To do so, we simply count the number of days of the considered period when the EDJ was detected at each grid point. These 2D EDJ frequency maps describe the local recurrence and preferred spatial configuration of the EDJ over the considered period and are expressed in percentage of time. The methodology has already been applied to examine the relationship between the EDJ and winter temperature extremes over Europe⁴³.

Definition of drivers of the future changes in EDJ

The metrics used in this study as drivers of the future changes in EDJ are collected from previous studies^{7,10,33}, which allow us to gather a set of remote factors that impact the NATL circulation. The climate change response of each driver is defined as the difference between the climatological mean metrics of the end of the 21st century (2069–2099) and the historical period (1979–2009). The drivers and associated metrics are defined as follows:

- Meridional temperature gradient at 200 hPa (Grad200): the difference between the polar ($[70^\circ\text{N}, 90^\circ\text{N}]$) and tropical ($[0^\circ, 20^\circ\text{N}]$) averages of the zonal mean temperature computed over the $[120^\circ\text{W}, 60^\circ\text{E}]$ domain at 200 hPa.
- Meridional temperature gradient at 850 hPa (Grad850): same as Grad200 but at 850 hPa.
- Stratospheric polar vortex (SPV): zonal mean zonal wind averaged between $[60^\circ\text{N}, 75^\circ\text{N}]$ at 10 hPa.
- Warming Hole (WH): SST averaged over $[35^\circ\text{N}, 60^\circ\text{N}; 40^\circ\text{W}, 10^\circ\text{W}]$.
- Zonal asymmetries in the equatorial Pacific SST: SST difference between the NIÑO4 $[5^\circ\text{S}, 5^\circ\text{N}; 160^\circ\text{E}, 150^\circ\text{W}]$ and the NIÑO3 $[5^\circ\text{S}, 5^\circ\text{N}; 150^\circ\text{W}, 90^\circ\text{W}]$ region.

The consideration of these phenomena as large-scale drivers of the EDJ latitude is supported by the literature. The direction of the relationship is clear for all of them, with the driver acting on the EDJ variability rather than the other way around. The thermodynamical drivers, namely, Grad200, Grad850 and WH affect the EDJ by modifying the NATL baroclinicity, which is the main source of variability of the NATL zonal wind. Grad200 is linked to (and largely modulated by) the TA, which induces EDJ shifts^{7,10,18,47}. Similarly, Grad850 is associated with the AA, which modifies the EDJ latitude^{17,18,20,21}. There are multiple causes behind AA (e.g. albedo and cloud feedbacks, changes in oceanic and atmospheric heat transport, modification of the surface type, etc.)²². The NATL WH is associated with the slow-down of the Atlantic Meridional Overturning Circulation (AMOC), which leads to reduced heating over the subpolar gyre region⁵⁴, changes in the meridional SST pattern, baroclinicity and ultimately, the EDJ latitude^{26,27}. The slow-down of the AMOC has been attributed to different factors, including the Greenland ice-sheet melting⁵⁵ and sea-ice loss in the polar regions⁵⁶. The NATL WH also influences the zonal gradient of near-surface air temperature across the NATL sector. Moving to the dynamical drivers (SPV), there exists mounting evidence about the effects of the SPV on the NATL EDJ⁴⁶, although the exact mechanism explaining the downward influence of the stratosphere on the troposphere is still not clear. Several studies have shown the potential impacts of future changes in SPV on the NATL tropospheric circulation^{30,32,33}. Finally, the zonal asymmetries of the equatorial Pacific SST are expected to increase their influence on the NATL circulation through the reinforcement of the atmospheric teleconnections^{10,34}. Additional drivers, such as the location of the NATL subtropical jet, the global near-surface temperature or the zonal 850 hPa temperature gradient in the NATL, were also analysed. However, they are not included in the presented analysis as they were not found independent from other drivers.

In addition to the large-scale drivers, we analyse whether future projections of the EDJ latitude are influenced by GCM biases (i.e., the ability of the GCM to capture present-day conditions). In particular, we focus on GCM biases in the EDJ latitude (Lat) regardless of the source leading to these biases. For each GCM, this bias is defined as the difference between the climatological means (1979–2009) of the Lat parameter obtained for the historical run and ERA5. EDJ Lat biases are computed for the two winter subseasons separately because they can exhibit intraseasonal variations (Fig. S3).

Multiple linear regression framework

The future change in the frequency pattern and parameters of the EDJ can be described as a linear combination of the drivers' responses to climate change. To find the leading drivers of the projected changes of the EDJ in the multimodel ensemble, we perform a multiple linear regression (MLR) similar to Zappa and Shepherd (2017)³³. The predicted variables are the future changes in the EDJ parameters (Eq. (1)) and in the 2D EDJ frequency field (Eq. (2)). In both cases, the predictors correspond to a vector constructed from the simulated climate change responses of that driver across the multimodel ensemble (each element of the vector represents the driver's response in one GCM). For instance, for the sample considering all GCMs, the changes in the EDJ latitude and the changes in the drivers' vectors have 21 elements, the number of GCMs that form the sample. Before building the regression models, the predictors and predicted variables were scaled by the global warming of each GCM, dividing them by the simulated change in the global surface temperature. This allows us to account for the different climate sensitivities across the multimodel ensemble:

$$\frac{\Delta \text{Param}_m}{\Delta \text{GW}_m} = a + \sum_{i=1}^6 b_i \left(\frac{\Delta \text{Driver}}{\Delta \text{GW}} \right)_{m,i} + \text{res} \quad (1)$$

$$\frac{\Delta \text{Freq}_{x,m}}{\Delta \text{GW}_m} = a_x + \sum_{i=1}^6 b_{x,i} \left(\frac{\Delta \text{Driver}}{\Delta \text{GW}} \right)_{m,i} + \text{res}_x \quad (2)$$

where the variables ΔParam , ΔFreq , ΔGW and ΔDriver are the changes between the future (2069–2099, SSP5–8.5) and present-day (1979–2009, historical) averages of the EDJ parameters, the 2D EDJ frequency field, the global mean surface temperature and the drivers, respectively. The coefficient a provides the response of the EDJ in the absence of drivers' changes, b_i gives the EDJ response to anomalies in the remote driver ΔDriver_i , and res represents residual variations not captured by the MLR. The suffixes m and x represent the GCM and the location in the longitude–latitude field. The MLR framework is applied to winter averages of the EDJ, as well as to the early and late winter subseasons, separately. The sign of EDJ frequency maps in Figs. 4 and 5 corresponds to that associated with the southward EDJ Lat Bias and the projections of the drivers detected in Fig. 3, i.e., a reinforcement of the negative Grad200, the intensification of the WH and a weakening of SPV.

The predictor selection is based on the computation of the p -value, which assesses the effect of the predictor candidate on the MLR model, following a stepwise procedure with forward selection and backward elimination. Starting with an empty MLR model, the predictors are added and removed sequentially, retaining those with significant ($p < 0.05$) non-zero coefficients and the smallest p -value. The process is repeated until adding and removing predictors do not improve the MLR model. This type of MLR model deals with the potential collinearity among predictors, because it includes only predictors that explain a significant additional fraction of the variance (provide independent information).

Model populations and statistics

We study the projected changes in the EDJ for different populations of GCMs. The first one is the full multimodel ensemble, which considers the 21 GCMs of Table S1. A second group only includes those GCMs that represent the climatological EDJ latitude sufficiently well for the 1979–2009 period. The purpose is to investigate if the projected changes depend or not on the ability of the GCMs to capture the mean EDJ features. The GCM bias is defined as the difference of the historical (1979–2009) monthly EDJ latitude climatology of each GCM minus that corresponding to the ERA5 reanalysis. The significance of the difference is assessed with a 1000-trial Monte Carlo at the 95% confidence level applied to the monthly series of EDJ latitudes (defined for early or late winter). Monthly series are computed from the daily values of EDJ latitude. The quantification of biases allows us to construct an ensemble of Neutral-GCMs, which comprise those with non-significant differences in the EDJ latitude with respect to ERA5 (Fig. S3b and d). The remaining GCMs, those that present a significantly biased EDJ Lat (Fig. S3a and c) are characterised by southward displaced EDJs with respect to ERA5.

For all of the diagnosed variables, the significance of the climate change signal, defined as the 30-yr mean state difference between the historical and SSP5–8.5 simulations, is tested using a Monte-Carlo test of 1000 realisations at the 95% confidence level. To do so, the projected change is tested against a 1000-sample distribution of differences between two randomly generated subsets. These subsets have the same number of cases as the historical and SSP5–8.5 but are generated by selecting random simulations from the total number of available experiments, namely, the 21 historical and SSP5–8.5 simulations.

Data availability

The ERA5 reanalysis data used in this study is publicly available at the Copernicus Climate Change Service Climate Data Store: <https://cds.climate.copernicus.eu/cdsapp#!/dataset/reanalysis-era5-pressure-levels?tab=form>. The CMIP6 data can be obtained from the ESGF website: <https://esgf-node.llnl.gov/projects/cmip6/>.

Code availability

The codes generated to develop this study are available upon request to the corresponding author.

Received: 22 January 2024; Accepted: 13 September 2024;

Published online: 04 October 2024

References

- Athanasiadis, P. J., Wallace, J. M. & Wettstein, J. J. Patterns of wintertime jet stream variability and their relation to the storm tracks. *J. Atmos. Sci.* **67**, 1361–1381 (2010).
- Maddison, J. W., Ayarzagüena, B., Barriopedro, D. & García-Herrera, R. Added value of a multiparametric eddy-driven jet diagnostic for understanding European air stagnation. *Environ. Res. Lett.* **18**, 084022 (2023).
- Mahlstein, I., Martius, O., Chevalier, C. & Ginsbourger, D. Changes in the odds of extreme events in the Atlantic basin depending on the position of the extratropical jet. *Geophys. Res. Lett.* **39**, 1–6 (2012).
- Barnes, E. A. & Polvani, L. Response of the midlatitude jets, and of their variability, to increased greenhouse gases in the CMIP5 models. *J. Clim.* **26**, 7117–7135 (2013).
- Hay, S. et al. Separating the influences of low-latitude warming and sea ice loss on Northern Hemisphere Climate change. *J. Clim.* **35**, 2327–2349 (2022).
- Oudar, T. et al. Robustness and drivers of the Northern Hemisphere extratropical atmospheric circulation response to a CO₂-induced warming in CNRM-CM6-1. *Clim. Dyn.* **54**, 2267–2285 (2020).
- Peings, Y., Cattiaux, J., Vavrus, S. J. & Magnusdottir, G. Projected squeezing of the wintertime North-Atlantic jet. *Environ. Res. Lett.* **13**, 074016 (2018).
- Shaw, T. A. Mechanisms of future predicted changes in the zonal mean mid-latitude circulation. *Curr. Clim. Chang. Rep.* **5**, 345–357 (2019).
- Barnes, E. A. & Polvani, L. M. CMIP5 projections of Arctic amplification, of the North American/North Atlantic circulation, and of their relationship. *J. Clim.* **28**, 5254–5271 (2015).
- Oudar, T., Cattiaux, J. & Douville, H. Drivers of the northern extratropical eddy-driven jet change in CMIP5 and CMIP6 models. *Geophys. Res. Lett.* **47**, 1–9 (2020).
- Dorrington, J., Strommen, K., Fabiano, F. & Molteni, F. CMIP6 models trend toward less persistent European blocking regimes in a warming climate. *Geophys. Res. Lett.* **49**, 1–12 (2022).
- Harvey, B. J., Cook, P., Shaffrey, L. C. & Schiemann, R. The response of the Northern Hemisphere storm tracks and jet streams to climate change in the CMIP3, CMIP5, and CMIP6 climate models. *J. Geophys. Res. Atmos.* **125**, 1–10 (2020).
- Ulbrich, U., Leckebusch, G. C. & Pinto, J. G. Extra-tropical cyclones in the present and future climate: a review. *Theor. Appl. Climatol.* **96**, 117–131 (2009).
- Harvey, B., Hawkins, E. & Sutton, R. Storylines for future changes of the North Atlantic jet and associated impacts on the UK. *Int. J. Climatol.* 1–18 <https://doi.org/10.1002/joc.8095> (2023).
- Peings, Y., Cattiaux, J., Vavrus, S. & Magnusdottir, G. Late twenty-first-century changes in the midlatitude atmospheric circulation in the CESM large ensemble. *J. Clim.* **30**, 5943–5960 (2017).
- Schiemann, R. et al. Northern Hemisphere blocking simulation in current climate models: evaluating progress from the Climate Model Intercomparison Project Phase 5 to 6 and sensitivity to resolution. *Weather Clim. Dyn.* **1**, 277–292 (2020).
- Barnes, E. A. & Simpson, I. R. Seasonal sensitivity of the Northern Hemisphere jet streams to Arctic temperatures on subseasonal time scales. *J. Clim.* **30**, 10117–10137 (2017).
- Butler, A. H., Thompson, D. W. J. & Heikes, R. The steady-state atmospheric circulation response to climate change-like thermal forcings in a simple general circulation model. *J. Clim.* **23**, 3474–3496 (2010).
- Deser, C., Tomas, R. A. & Sun, L. The role of ocean–atmosphere coupling in the zonal-mean atmospheric response to Arctic sea ice loss. *J. Clim.* **28**, 2168–2186 (2015).

20. Oudar, T. et al. Respective roles of direct GHG radiative forcing and induced Arctic sea ice loss on the Northern Hemisphere atmospheric circulation. *Clim. Dyn.* **49**, 3693–3713 (2017).
21. Screen, J. A. et al. Consistency and discrepancy in the atmospheric response to Arctic sea-ice loss across climate models. *Nat. Geosci.* **11**, 155–163 (2018).
22. Taylor, P. C. et al. Process drivers, inter-model spread, and the path forward: a review of amplified Arctic warming. *Front. Earth Sci.* **9**, 1–29 (2022).
23. O’Gorman, P. A. & Singh, M. S. Vertical structure of warming consistent with an upward shift in the middle and upper troposphere. *Geophys. Res. Lett.* **40**, 1838–1842 (2013).
24. Woollings, T., Drouard, M., O’Reilly, C. H., Sexton, D. M. H. & McSweeney, C. Trends in the atmospheric jet streams are emerging in observations and could be linked to tropical warming. *Earth Environ.* **4**, 125 (2023).
25. Xie, S. Ocean warming pattern effect on global and regional climate change. *AGU Adv.* **1**, (2020).
26. Gervais, M., Shaman, J. & Kushnir, Y. Impacts of the North Atlantic warming hole in future climate projections: mean atmospheric circulation and the North Atlantic jet. *J. Clim.* **32**, 2673–2689 (2019).
27. Bellomo, K., Angeloni, M., Corti, S. & von Hardenberg, J. Future climate change shaped by inter-model differences in Atlantic meridional overturning circulation response. *Nat. Commun.* **12**, 3659 (2021).
28. Harvey, B. J., Shaffrey, L. C. & Woollings, T. J. Deconstructing the climate change response of the Northern Hemisphere wintertime storm tracks. *Clim. Dyn.* **45**, 2847–2860 (2015).
29. Woollings, T., Gregory, J. M., Pinto, J. G., Reyers, M. & Brayshaw, D. J. Response of the North Atlantic storm track to climate change shaped by ocean-atmosphere coupling. *Nat. Geosci.* **5**, 313–317 (2012).
30. Maycock, A. C., Masukwedza, G. I. T., Hitchcock, P. & Simpson, I. R. A regime perspective on the north Atlantic eddy-driven jet response to sudden stratospheric warmings. *J. Clim.* **33**, 3901–3917 (2020).
31. Afargan-Gerstman, H. & Domeisen, D. I. V. Pacific modulation of the North Atlantic storm track response to sudden stratospheric warming events. *Geophys. Res. Lett.* **47**, 1–10 (2020).
32. Manzini, E., Karpechko, A. Y. & Kornbluh, L. Nonlinear response of the Stratosphere and the North Atlantic-European climate to global warming. *Geophys. Res. Lett.* **45**, 4255–4263 (2018).
33. Zappa, G. & Shepherd, T. G. Storylines of atmospheric circulation change for European regional climate impact assessment. *J. Clim.* **30**, 6561–6577 (2017).
34. Beverley, J. D., Collins, M., Lambert, F. H. & Chadwick, R. Drivers of changes to the ENSO–Europe teleconnection under future warming. *Geophys. Res. Lett.* **51**, 1–9 (2024).
35. Ciasto, L. M., Li, C., Wettstein, J. J. & Kvamstø, N. G. North Atlantic storm-track sensitivity to projected sea surface temperature: local versus remote influences. *J. Clim.* **29**, 6973–6991 (2016).
36. Abid, M. A. et al. Separating the Indian and Pacific Ocean impacts on the Euro-Atlantic response to ENSO and its transition from early to late winter. *J. Clim.* **34**, 1531–1548 (2021).
37. Herceg-Bulić, I., Ivačić, S. & Popović, M. Impact of tropical SSTs on the late-winter signal over the North Atlantic-European region and contribution of midlatitude Atlantic. *npj Clim. Atmos. Sci.* **6**, 172 (2023).
38. Ayarzagüena, B., Ineson, S., Dunstone, N. J., Baldwin, M. P. & Scaife, A. A. Intraseasonal effects of El Niño–Southern Oscillation on North Atlantic climate. *J. Clim.* **31**, 8861–8873 (2018).
39. Sung, M. K., Ham, Y. G. & Kug, J. S. & An, S. II. An alternative effect by the tropical North Atlantic SST in intraseasonally varying El Niño teleconnection over the North Atlantic. *Tellus Ser. A Dyn. Meteorol. Oceanogr.* **65**, 1–13 (2013).
40. Cassou, C. Intraseasonal interaction between the Madden–Julian Oscillation and the North Atlantic Oscillation. *Nature* **455**, 523–527 (2008).
41. Bracegirdle, T. J., Lu, H. & Robson, J. Early-winter North Atlantic low-level jet latitude biases in climate models: implications for simulated regional atmosphere–ocean linkages. *Environ. Res. Lett.* **17**, 014025 (2022).
42. Barriopedro, D., Ayarzagüena, B., García-Burgos, M. & García-Herrera, R. A multi-parametric perspective of the North Atlantic eddy-driven jet. *Clim. Dyn.* **61**, 375–397 (2023).
43. García-Burgos, M., Ayarzagüena, B., Barriopedro, D. & García-Herrera, R. Jet configurations leading to extreme winter temperatures over Europe. *J. Geophys. Res. Atmos.* **128**, e2023JD039304 (2023).
44. Woollings, T., Hannachi, A. & Hoskins, B. Variability of the North Atlantic eddy-driven jet stream. *Q. J. R. Meteorol. Soc.* **136**, 856–868 (2010).
45. Lorenz, D. J. & DeWeaver, E. T. Tropopause height and zonal wind response to global warming in the IPCC scenario integrations. *J. Geophys. Res. Atmos.* **112**, 1–11 (2007).
46. Butchart, N. The stratosphere: a review of the dynamics and variability. *Weather Clim. Dyn.* **3**, 1237–1272 (2022).
47. Peings, Y., Cattiaux, J. & Magnusdottir, G. The polar stratosphere as an arbiter of the projected tropical versus polar tug of war. *Geophys. Res. Lett.* **46**, 9261–9270 (2019).
48. Baker, H. S., Woollings, T. & Mbengue, C. Eddy-driven jet sensitivity to diabatic heating in an idealized GCM. *J. Clim.* **30**, 6413–6431 (2017).
49. Baker, H. S., Mbengue, C. & Woollings, T. Seasonal sensitivity of the Hadley cell and cross-hemispheric responses to diabatic heating in an idealized GCM. *Geophys. Res. Lett.* **45**, 2533–2541 (2018).
50. Davini, P. & D’Andrea, F. From CMIP3 to CMIP6: Northern hemisphere atmospheric blocking simulation in present and future climate. *J. Clim.* **33**, 10021–10038 (2020).
51. Rousi, E., Kornhuber, K., Beobide-Arsuaga, G., Luo, F. & Coumou, D. Accelerated western European heatwave trends linked to more-persistent double jets over Eurasia. *Nat. Commun.* **13**, 1–11 (2022).
52. Eyring, V. et al. Overview of the Coupled Model Intercomparison Project Phase 6 (CMIP6) experimental design and organization. *Geosci. Model Dev.* **9**, 1937–1958 (2016).
53. Hersbach, H. et al. The ERA5 global reanalysis. *Q. J. R. Meteorol. Soc.* **146**, 1999–2049 (2020).
54. Liu, W., Fedorov, A. V., Xie, S. P. & Hu, S. Climate impacts of a weakened Atlantic meridional overturning circulation in a warming climate. *Sci. Adv.* **6**, 1–8 (2020).
55. Weijer, W., Maltrud, M. E., Hecht, M. W., Dijkstra, H. A. & Klinkhous, M. A. Response of the Atlantic Ocean circulation to Greenland Ice Sheet melting in a strongly-eddy ocean model. *Geophys. Res. Lett.* **39**, 1–6 (2012).
56. Sévellec, F., Fedorov, A. V. & Liu, W. Arctic sea ice decline weakens the Atlantic Meridional Overturning Circulation. *Nat. Clim. Chang.* **7**, 604–610 (2017). (8).

Acknowledgements

This research was funded by the JeDis (RTI2018-096402-B-I00) project. Also supported by the Grant PRE2019-090618 from Spanish Ministerio de Ciencia e Innovación.

Author contributions

M.G.-B. performed computational analysis and the writing of the original draft of the paper. B.A., T.W., D.B., R.G.-H. and M.G.-B. contributed to the conceptualisation, the development of the methodology and writing of the paper. They also have read and approved the manuscript.

Competing interests

The authors declare no competing interests.

Additional information

Supplementary information The online version contains supplementary material available at

<https://doi.org/10.1038/s41612-024-00775-2>.

Correspondence and requests for materials should be addressed to Marina García-Burgos.

Reprints and permissions information is available at

<http://www.nature.com/reprints>

Publisher's note Springer Nature remains neutral with regard to jurisdictional claims in published maps and institutional affiliations.

Open Access This article is licensed under a Creative Commons Attribution-NonCommercial-NoDerivatives 4.0 International License, which permits any non-commercial use, sharing, distribution and reproduction in any medium or format, as long as you give appropriate credit to the original author(s) and the source, provide a link to the Creative Commons licence, and indicate if you modified the licensed material. You do not have permission under this licence to share adapted material derived from this article or parts of it. The images or other third party material in this article are included in the article's Creative Commons licence, unless indicated otherwise in a credit line to the material. If material is not included in the article's Creative Commons licence and your intended use is not permitted by statutory regulation or exceeds the permitted use, you will need to obtain permission directly from the copyright holder. To view a copy of this licence, visit <http://creativecommons.org/licenses/by-nc-nd/4.0/>.

© The Author(s) 2024